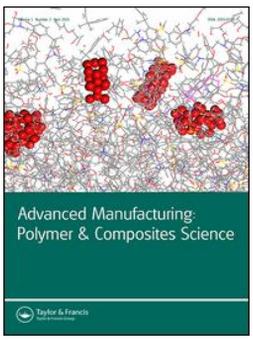

Taylor & Francis
Taylor & Francis Group

Advanced Manufacturing: Polymer & Composites Science

ISSN: (Print) (Online) Journal homepage: https://www.tandfonline.com/loi/yadm20

Permeability of co-cured honeycomb sandwich skins: effect of gas transport during processing

Trisha Palit , Timotei Centea , Mark Anders , Daniel Zebrine & Steven Nutt

To cite this article: Trisha Palit , Timotei Centea , Mark Anders , Daniel Zebrine & Steven Nutt (2020): Permeability of co-cured honeycomb sandwich skins: effect of gas transport during processing, Advanced Manufacturing: Polymer & Composites Science, DOI: 10.1080/20550340.2020.1802685

To link to this article: https://doi.org/10.1080/20550340.2020.1802685

Published online: 07 Aug 2020.

ADVANCED MANUFACTURING: POLYMER & COMPOSITES SCIENCE
https://doi.org/10.1080/20550340.2020.1802685

Permeability of co-cured honeycomb sandwich skins: effect of gas transport during processing

Trisha Palit, Timotei Centea, Mark Anders, Daniel Zebrine and Steven Nutt

M.C. Gill Composites Center, Viterbi School of Engineering, University of Southern California, Los Angeles, CA, USA

ABSTRACT

Potential links between pressure conditions during co-cure of honeycomb sandwich panels, the extent of gas flow through facesheet and bond-line, and the level of permeability in the cured skin were evaluated. Half-sandwich structures comprised of fiber-reinforced polymer facesheets, film adhesive, and core were fabricated using a custom-built lab fixture. Autoclave, bag, and core pressures were varied to produce controlled, constant pressure differences during cure, and the resulting skins were tested for permeability using a fixture constructed to measure gas flow rate across the skins and to locate gas flow pathways. Facesheet cross-sections were analyzed to evaluate porosity. Porosity and the number of gas flow pathways were correlated to permeability, but significant gas flow was possible without high void content or with few channels, as pressure differentials led to complex variations in permeability. Overall, the study provides new insights into gas transport during composites processing and manufacturing, and the results provide guidance for modifying manufacturing processes to ensure part quality.

KEYWORDS

Co-cure; honeycomb; prepreg; permeability; sandwich structures; composites manufacturing

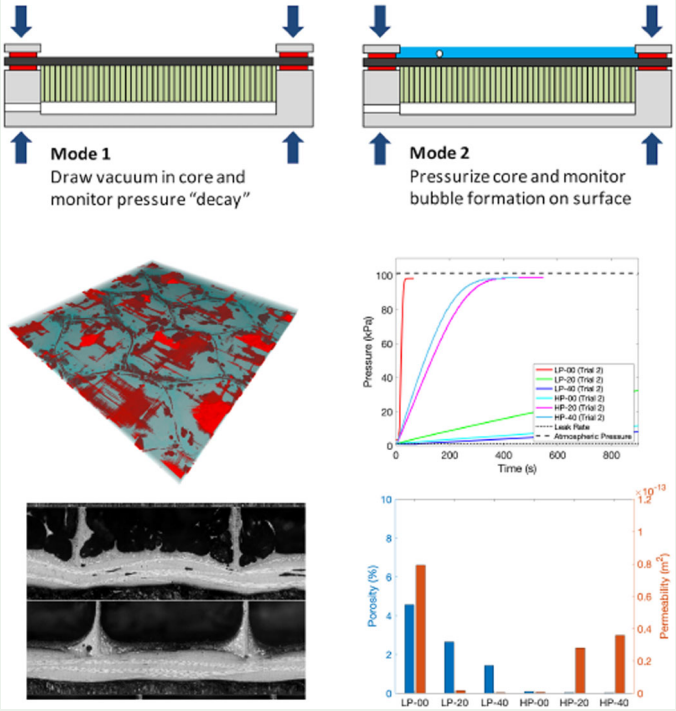

1. Introduction

In this work, the relationships between process conditions and cured skin permeability in honeycomb sandwich panels are described. Specifically, experiments focus on evaluating the potential links between pressure conditions during co-cure (autoclave pressure [P_a], bag pressure [P_b], and core pressure [P_c]), the extent of gas flow through facesheet and bond-line, the permeability in the cured skin, and micro-structural defects such as porosity. To date, the relationship between skin permeability after cure, gas transport factors, and microstructural defects has not been studied in detail. Understanding this relationship can inform adjustments to co-cure manufacturing processes to

CONTACT Trisha Palit tpalit@usc.edu; trisha.palit@gmail.com 3335 S. Figueroa St. Apt 349A, Los Angeles, CA 90007, USA

produce parts with specified permeability levels. Such insights are especially important in the aerospace industry, where permeability can allow fluids to degrade the core and polymers. This damage can potentially lead to issues in service due to decreased structural integrity [1, 2].

Sandwich structures composed of fiber-reinforced facesheets, an adhesive bond-line, and a low-density core, are important to industries where high specific mechanical strength and stiffness are required, including aerospace, wind energy, and others [2]. These structures are particularly well-suited to applications involving flexural or surface loads and offer additional options for acoustic and thermal insulation. Typically, the facesheets consist of a fiber-reinforced polymer laminate (e.g. carbon epoxy), while the adhesive is supplied as a thermoset polymer film. The honeycomb core most often consists of metallic (aluminum) or aramid cells (Nomex dipped in phenolic) arranged in a periodic hexagonal array [2].

Sandwich structures can be produced via secondary bonding or via co-cure. Secondary bonding involves bonding pre-cured prepreg laminate facesheets to a low-density core insert using film adhesive. Alternatively, prepreg facesheets and film adhesives can be cured in a single step directly onto the low-density core, a process known as co-cure [2]. During co-cure, prepreg plies, film adhesive layers, and a core insert are laid up to form a sandwich structure, which is then vacuum-bagged and cured in an autoclave or oven. This process enables production of large structures with complex features, for which other manufacturing approaches (e.g. bonding after cure) would be challenging because of difficulties maintaining dimensional tolerances. However, interactions between process phenomena associated with the facesheet, adhesive, and core constituents render co-cure more complex than secondary bonding and can thus introduce defects in manufactured parts.

The aerospace industry requires high levels of structural integrity and reliability. Therefore, defects arising from the manufacture of honeycomb sandwich structures must be minimized. Defects include porosity in the facesheet and/or adhesive bond-line, unintentional distortion of the specified shape of the part, and delamination and cracks [3]. These defects can be difficult to detect visually, but are more readily revealed using a microscope to image facesheet and bondline cross-sections, revealing the microstructure of the skins. Furthermore, the sandwich skins (facesheets and adhesive bond-lines) must be impermeable to fluids to prevent ingress of moisture and solvents, which can degrade the core and polymers and potentially reduce structural integrity [1]. However, skin permeability can be affected by process-induced porosity. During co-cure, porosity can arise due to void growth within the facesheet or adhesive, and due to resin starvation caused by resin bleed into core cells. Furthermore, gas flow pathways can form within the skin due to core and bag pressure differences. Overall, this relationship between cured skin permeability, process-induced microstructural defects, and gas transport factors has not been studied in detail.

1.1. Background

Permeability is defined as the capacity for fluid flow through a porous material, and can be calculated from a measured flow rate, a pressure gradient, and information about the medium geometry and properties. Assuming homogeneity across a cured prepreg, Darcy's Law can be used to calculate the transverse air permeability [4]. In the 1-D form of Darcy's Law, Q is the volumetric flow rate, K is permeability, A is the cross-sectional area through which the fluid flows, μ is the viscosity of the fluid, and dP/dL is the pressure gradient across the porous medium:

$$Q = \frac{KA}{\mu}\frac{dP}{dL} \tag{1}$$

Alternately, the permeability can be estimated using a pressure equilibration method, which is appropriate for materials of low permeability [5, 6]. If the porous medium is bounded by a "reservoir" of known volume on one side and a medium with constant pressure (different from the initial reservoir pressure) on the other, the pressure within the reservoir during pressure evolution can be monitored and used to compute permeability. In such cases, Darcy's Law can be expressed according to Equation (2), where P_b is the bag pressure, P_c is the core pressure at time t, $P_{c,i}$ is the initial core pressure at $t = 0$ min, and V_{CORE} is the volume of air on the honeycomb core side of the skin. The permeability, K, can be calculated by plotting the left-hand side of the equation versus time and estimating the slope to provide an average value over time.

$$ln\frac{(P_b + P_{c,i})(P_b - P_c)}{(P_b - P_{c,i})(P_b + P_c)} = -\frac{KAP_b}{L\mu V_{CORE}}t \tag{2}$$

Generally, the permeability of a porous medium depends on multiple factors, including porosity (ratio of pore volume to total volume), pore connectivity, and tortuosity of the gas flow pathways [7]. Higher permeabilities cause increased gas flow rates.

Sandwich skins must be impermeable for most applications, yet permeability often arises in practice as a manufacturing defect. Permeability of prepregs during cure of sandwich structures can be

challenging to determine analytically because multiphase flow causes deviations from Darcy's Law. Using an empirical falling pressure method to measure permeability during cure, Tavares et al. [8, 9] reported that permeability depended on resin viscosity evolution. As viscosity decreases during cure, resin flows through natural passages in the fiber bed and ply pathways. The character of these pathways depends on the type of fabric and weave pattern, and these characteristics affect permeability, as reported by Kratz et al. [6, 7]. Resin flow can occlude these pathways, decreasing gas flow and permeability. As the cure cycle progresses, viscosity drops, resin fills air passages, and permeability stabilizes as resin viscosity then increases to the point of gelation. Kratz et al. reported an increase in permeability after resin gelation, which they attributed either to matrix shrinkage or microcracking. They observed matrix microcracking and attributed it to the small part surface, but they asserted it would not be a factor in larger parts. However, microcracking can increase gas permeability, as reported by Grenoble after conducting fatigue tests on cured laminates [10].

Permeable skins can also stem from porosity, a type of defect that can be readily quantified. Void formation during processing of composite prepregs is well-understood, and occurs because the applied pressure (and, hence, resin pressure) is insufficient to collapse gas bubbles. Such bubbles can be caused by air entrapped between plies during lay-up, air entrained in the prepreg matrix before cure, or volatiles released by the polymer during cure [8, 9]. During co-cure of sandwich structures, porosity can also arise because gas entrapped within the core can travel through the skins. Tavares et al. [5, 11–14] and Kratz et al. [1, 6, 15–19] conducted multiple studies on gas transport during co-cure of honeycomb sandwich structures, showing that core pressure during processing strongly affects skin quality. Additional work is required to accurately quantify the complex relationship between core pressure and skin porosity.

Control of pressure in the core can also be affected by the venting or sealing of the core. If the core is vented, air trapped in the core during layup has a direct pathway to escape the external environment. The pressure in the core will then equal the pressure of the external environment. Vented core is often employed in situations where core pressure buildup could damage the structure, such as during spacecraft launch [20–22]. Venting can be achieved by perforating the core through the cell walls and through a pre-cured, tool-side skin with holes. Vented configurations can be used to control pressure in the core during the cure process. Vented core also prevents pressure gradients within the core, ensuring a uniform pressure distribution [21]. Alternatively, if the core is sealed, air cannot escape through a direct pathway to the environment. Gas transport instead depends on skin permeability, thermal expansion of gases, and core and bag pressure differences. In such cases, the core pressure will vary with external temperature and pressure changes throughout the curing process, and is more difficult to measure and precisely control.

Effective skin permeability also evolves as the prepreg facesheet consolidates and film adhesive flows at the bond-line. During co-cure, core air can flow through the skins by displacing liquid resin and forming channels. If these egress channels remain in the skin after cure is complete, the resulting skin will be permeable to gases during subsequent service. This possible relationship between processing and cured skin permeability was described in a study by Kratz and Hubert [12], who showed that a panel in which core pressure was changing at resin gelation (indicating that gas evacuation through the skins was occurring) had a greater permeability after cure than a comparable panel for which the core pressure was stable at gelation (indicating no gas evacuation).

Pressure in the vacuum bag can also influence defect formation as much as pressure in the core. Anders et al. [21] conducted experiments on a part using positive pressure in the bag and an equilibrated core to suppress the formation of defects. A one-hour, room-temperature vacuum de-bulk allowed the evacuation of gases from within the facesheet while the resin viscosity was relatively high because of low temperatures. Once temperatures were increased and resin had filled the empty spaces within and between the plies, in-bag pressurization increased resin pressure. The pressure ensured that gases remained dissolved in the resin. Furthermore, equilibration between the bag and core created a hydrostatic pressure condition at the facesheet boundaries that prevented gases from being driven through the skin and forming voids. This combination of conditions resulted in low porosity. A part made using in-bag pressurization was directly compared to an equivalent part produced without in-bag pressurization but with equilibrated core. In the latter part, the reduced pressures did not suppress the release of dissolved volatiles, allowing more voids to form. While in-bag pressurization deviates from conventional autoclave methods, the practice was developed for the US Air Force in the 1980s and is industrially relevant [23]. This method was studied previously with respect to the effects on defect formation, but the effects of in-bag pressurization on cured permeability have not been studied [21].

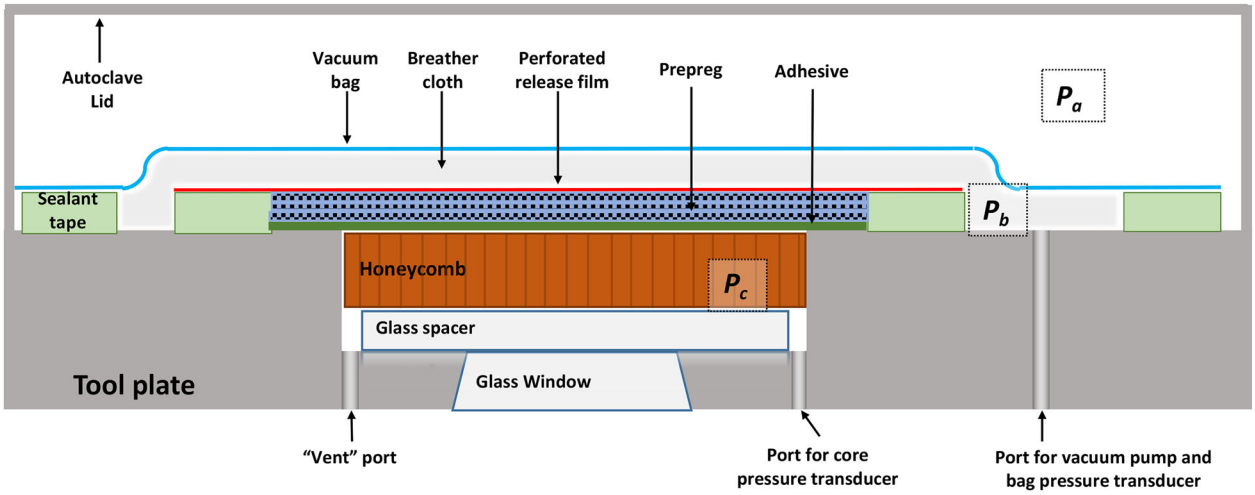

Figure 1. A schematic of the mini-autoclave test fixture.

1.2. Objectives

The specific goals of this study were to:

1. clarify the effect of gas transport factors (flow rate, pressure difference) during processing on permeability of autoclave co-cured skins,
2. develop the relationship between microstructural characteristics of co-cured skins and their permeability in the cured state, and
3. formulate manufacturing guidelines for producing impermeable facesheets.

Our approach consisted of fabricating honeycomb panels under various co-cure conditions, measuring the permeability of the cured skins, and analyzing the microstructures of the cured parts using microscopy and X-ray computed tomography. The results show that processing conditions affect cured skin permeability, and that the rate of gas flow through cured skins relates to the microstructural quality of the facesheet laminate and bond-line. Insights gained from the study can be used to design effective co-cure processes, as well as to support quality assurance by identifying parts in which processing may lead to skin permeability.

2. Experimental procedures

Parts were fabricated under controlled pressure conditions. Two baseline conditions with equilibrated core were used: low pressure (designed to induce defect formation), and high pressure (intended to suppress void formation). Furthermore, variations on each baseline were performed by imposing a constant pressure difference (ΔP) between bag and core. Pressure differences were imposed to achieve different gas flow rates between the bag and core. The fabricated parts were then tested, including cured permeability measurements (using a bespoke test fixture) and microstructural analysis of polished cross-sections. These datasets identified possible relationships between pressure conditions during processing, microstructural characteristics, and cured permeability.

2.1. Materials

Material characterization was performed on selected prepreg, adhesive, and core. An aerospace-grade plain-weave prepreg was used (HexPly® AGP193PW/8552S provided by the Hexcel Corporation). The prepreg consisted of carbon fibers (AS4), 193 g/m^2 fiber areal weight, 3000 fibers per tow, and was fully saturated to 38% by weight with toughened epoxy resin (8552S). The prepreg was produced via a solvated tower process [24]. A film adhesive was used (Henkel Loctite® EA 9658AERO NWG) [25], along with a honeycomb core (Nomex-based HD132 with 1/8" cells from the Gill Corporation).

2.2. Methods

2.2.1. Part fabrication

Honeycomb core panels were fabricated using a lab-scale instrumented test fixture designed to replicate industrial autoclave conditions while allowing detailed analysis of processing [14]. All panels were half-sandwich structures consisting of the bag-side skin and core. The bag-side skin consisted of four plies of prepreg, and the tool-side skin was not included. A schematic of the test fixture used (referred to as a mini-autoclave) is shown in Figure 1, and described elsewhere [14]. The base consists of a flat tool plate with a machined pocket. The pocket contains a window and a glass spacer, which support the curing part and allow real-time visual observation. For autoclave cure, the base was overlaid with a lid that allows pressurization of the gas outside the bag (P_a) to 377 kPa, or 40 psig.

Temperature was controlled using integrated resistive heaters and monitored at multiple locations. Finally, gas pressures within the core, bag, and autoclave volumes were controlled and measured independently. High-temperature pressure sensors (Omega Engineering PX32B1) were used to measure pressures in the bag and core. For all parts tested, the thermal cycle consisted of a 1 h room-temperature vacuum hold followed by a 1 h hold at 110 °C and a 2 h hold at 177 °C, with 2 °C/min heat-up and cool-down ramps throughout. Different pressure cycles were used for different parts, as specified in Table 1. Two categories of parts were fabricated: 1) low-pressure (LP) parts in which the pressure in the bag was 0 kPa, nominally (<5 kPa) and 2) high-pressure (HP) parts in which the bag pressure was 239 kPa. Within these two categories, three pressure gradients between the bag and core pressures were tested (0 kPa, 20 kPa, and 40 kPa), the core pressure being greater. Two samples were produced and tested for each pressure gradient case, with samples grouped into Trial 1 and Trial 2. While the conditions in Trial 1 and Trial 2 were the same, the results exhibited different trends, making trial groupings valuable for discussion. Additionally, pressure in the core for the high-pressure parts tended to vary slightly due to the configuration of the curing process. These pressures are marked as approximate in Table 1.

2.2.2. Cured permeability testing

To measure the permeability of cured skins, a custom-machined permeability test fixture consisting of a metal block with a pocket designed to contain the honeycomb core (similar to the mini-autoclave) and a clamping frame was fabricated (Figure 2). When setting up a test, the honeycomb panel was inserted into the metal block, and the frame was clamped over the skin. O-rings sealed the skin-block and skin-frame interfaces. The pressure in the cavity was measured using a high-temperature pressure sensor (Omega Engineering PX32B1) and was controlled through a port on the side of the fixture. The leak rate of the fixture was minimized by the simplicity of the design, as well as by careful assembly of all threaded components and use of liquid thread sealant, and measured by placing an impermeable metal plate between the block and clamping frame O-rings. When used appropriately, the fixture restricted gas migration to through-thickness flow across the skin.

Permeability of the cured skin was measured using two modes of operation. In Mode 1, vacuum was drawn in the core, and the cavity was then isolated from the pump. A pressure sensor was used to measure the subsequent pressure equilibration to atmospheric pressure. As the core pressure increased because of inflow of air from the atmosphere through the skin, the pressure versus time data was recorded. The data was used in Equation (2) to calculate permeability K. Tests continued until the core pressure reached ambient, or for a maximum duration of 15 min. The leak rate of the fixture was measured using a thin metal plate, considered to be impermeable, in place of a facesheet in the fixture. The permeability associated with the leak rate of the fixture when testing an impermeable surface is considered to be the minimum permeability detectable with the fixture. In Mode 2, the frame was filled with water, and positive pressure (~170 kPa, or 10 psig) was introduced into the core, forcing air through the skin and leading to bubble formation within the water. This mode of operation allowed the locations of the gas flow channels to be revealed. During Mode 2 testing, a video camera in a fixed position was used to record locations of bubble formation. As bubbles formed, a trace was performed over the images to record the relative position on the facesheet.

Table 1. Test matrix.

Case	Description	P_a (kPa)	P_b (kPa)	P_c (kPa)
LP-00	$\Delta P = 0$ kPa (Baseline Part)	377	0	0
LP-20	$\Delta P = 20$ kPa	377	0	~20
LP-40	$\Delta P = 40$ kPa	377	0	~40
HP-00	$\Delta P = 0$ kPa (In-Bag Pressurization)	377	239	239
HP-20	$\Delta P = 20$ kPa (In-Bag Pressurization)	377	239	~259
HP-40	$\Delta P = 40$ kPa (In-Bag Pressurization)	377	239	~279

2.2.3. Microstructural analysis

The microstructural characteristics of each facesheet were assessed from polished sections. Two samples (50 mm × 25 mm) were cut from each facesheet along a row of core cell centers (Figure 3), polished, and imaged using a digital stereo microscope (Keyence

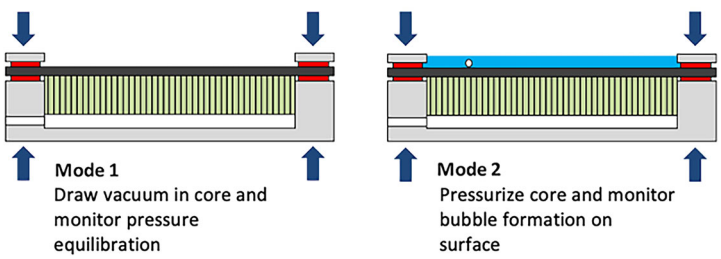

Figure 2. Cured permeability testing fixture: operation in Mode 1 and Mode 2.

VHX-600). Sides A and B refer to the left and right side of a single row of center core cells, as illustrated in Figure 3. Facesheet porosity (and other statistical information, e.g. average and maximum pore sizes) was calculated from the resulting images using the ratio of total void area to total cross-sectional area. Dimpling and fillet quality were also observed as indicators of part quality. Select samples were imaged using X-ray computed tomography, with a focus on the 100 mm^2 area of one or two isolated gas evacuation pathways. An X-ray system was used (Phoenix X-ray) with a voxel size of 37.03 μm^3.

Table 2. Cured permeability, channel number, and porosity values.

Trial	Case	Permeability (m^2)	Channels	Porosity (%)
1	LP-00	5.89E-14	17	6.02
	LP-20	3.96E-15	8	2.36
	LP-40	4.09E-15	10	3.63
	HP-00	9.96E-18	0	0.14
	HP-20	3.63E-17	0	0.11
	HP-40	1.06E-14	3	0.11
2	LP-00	7.93E-14	22	4.57
	LP-20	1.76E-15	2	2.65
	LP-40	4.19E-16	1	1.43
	HP-00	6.25E-16	0	0.09
	HP-20	2.81E-14	2	0.03
	HP-40	3.59E-14	2	0.02

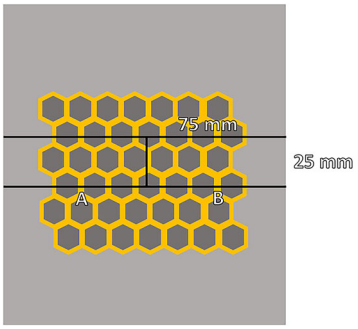

Figure 3. Schematic of microscopy samples (A and B) extracted from each honeycomb panel.

3. Results and discussion

A summary of numerical results including permeability, number of channels, and porosity for each sample can be found in Table 2.

3.1. Part fabrication

The pressure and temperature data shown in Figure 4 provides representative profiles of experiments performed with no pressure gradients for both the low-pressure, LP-00, and high-pressure case, HP-00. For experiments with pressure gradients of 20 kPa or 40 kPa, the core pressure was, respectively, 20 kPa or 40 kPa greater than the bag pressure.

3.2. Cured permeability testing

The pressure equilibration data shown in Figure 5 were used in Equation (2) to determine permeability values. The minimum permeability caused by the leak rate of the fixture was determined to be 5.8×10^{-18} m^2. When discussing low permeability values, values are compared to this lower bound.

The values in Figure 6 display notable trends. Within Trial 1, the LP-00 sample showed the greatest permeability, and HP-00 exhibited the lowest permeability, which was only two times greater than the minimum permeability. This result was consistent with in-bag pressurization processing conditions expected to eliminate the chance for flow through the skins and to reduce porosity. The permeability of sample LP-00 was approximately 6000 times greater than sample HP-00, indicating that process conditions caused a marked difference. The LP-20 and LP-40 skins exhibited virtually identical permeabilities and were 15 times less permeable than the sample LP-00. Increasing the pressure gradient from 0 kPa to 20 kPa decreased permeability, but further

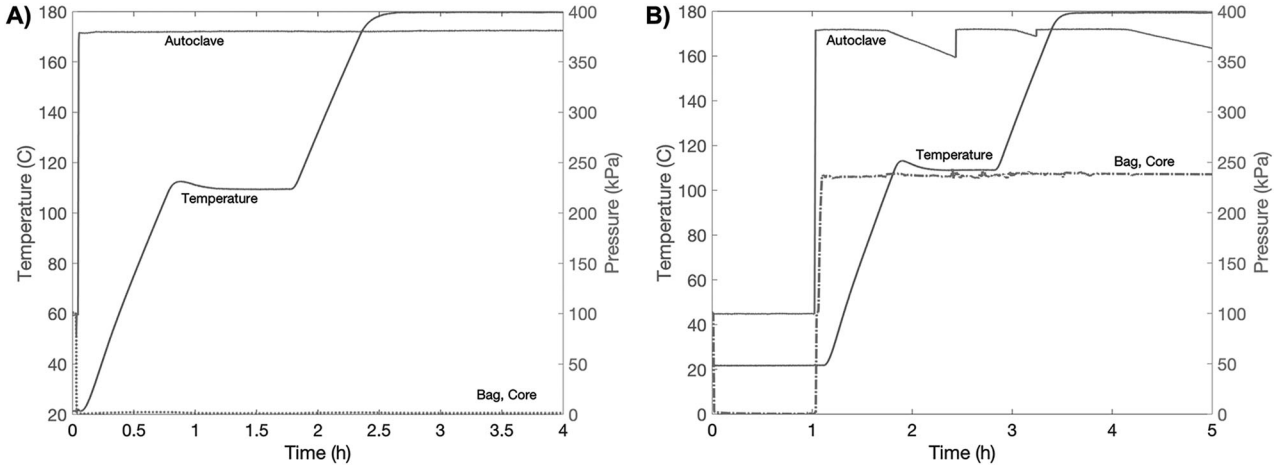

Figure 4. Measured data for representative co-cure experiments for (A) low-pressure and (B) high-pressure cases with no pressure gradient.

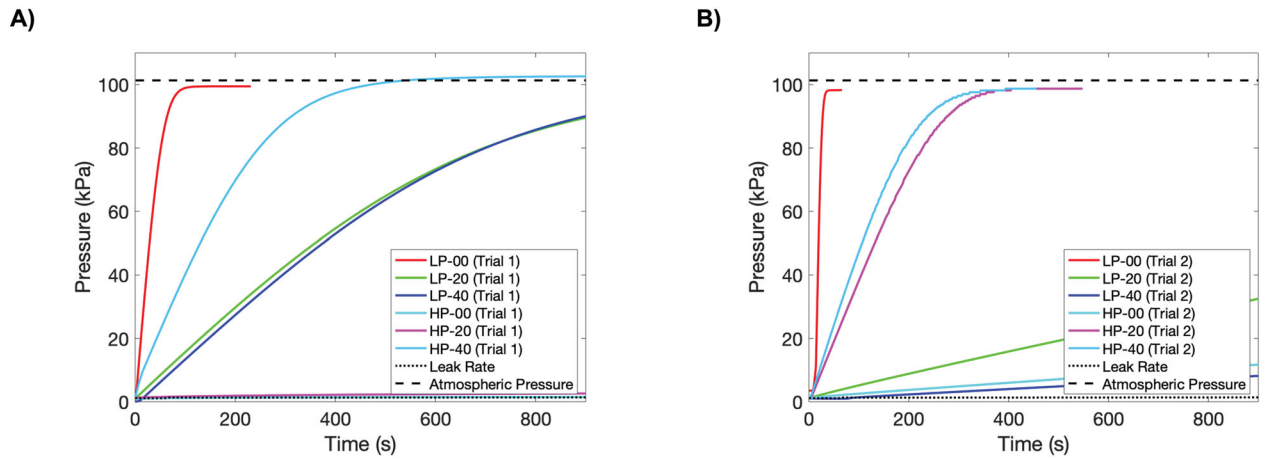

Figure 5. Pressure equilibration over time for (A) Trial 1 and (B) Trial 2 as measured by the permeability fixture.

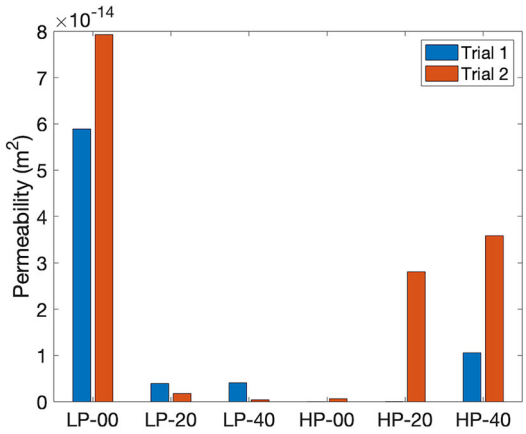

Figure 6. Permeability values for Trials 1 and 2.

increasing the gradient past 20 kPa had little effect. However, the HP series behaved differently — a larger pressure gradient increased permeability as opposed to decreasing it. Increasing the gradient from 0 kPa to 20 kPa resulted in a four-fold increase in permeability, while increasing the gradient from 20 kPa to 40 kPa resulted in a 300-fold increase.

In Trial 2, the various pressure gradients caused similar overall permeability effects. However, while overall trends were preserved, repeated pressure conditions did not consistently produce the same permeability values. Notably, the highest permeability values again occurred under LP-00 conditions and a low permeability value occurred under HP-00 conditions. LP-40 also produced a low permeability value, which was not seen in Trial 1. However, values for these pressure conditions varied from the permeability values under the same conditions in Trial 1, with values approximately 100 times the minimum fixture leak value. Within the LP series, increasing the pressure gradient again decreased permeability. Increasing the pressure gradient from 0 kPa to 20 kPa decreased permeability by a factor of 50, and increasing the gradient from 20 to 40 kPa further decreased permeability by a factor of four. Within the HP series, increasing the pressure gradient *increased* permeability. Raising the pressure gradient from 0 kPa to 20 kPa increased permeability by a factor of 45, while increasing the gradient from 20 kPa to 40 kPa resulted in little further change.

These permeability measurements indicate that low pressures with no pressure gradient can result in large permeability values, while in-bag pressurization with no pressure gradient can consistently result in low permeability values. Within the low-pressure series and the high-pressure series, two different trends were observed in response to increasing core pressure and the pressure gradient. In the low-pressure series, increasing core pressure decreased permeability values. In contrast, for the high-pressure series, increasing the pressure gradient increased permeability. However, the threshold pressure gradient value at which permeability increased cannot be well determined from this data. In Trial 1, this threshold point was between 20 and 40 kPa, while in Trial 2 the point was between 0 and 20 kPa. This difference indicates variability in the mechanism responsible for permeability, even under consistent pressures, or variability in the materials used, especially when considering alignment of pinholes in woven fabric. Further trials are required to more accurately quantify the threshold value and to better understand the process. However, the number of trials conducted here suffices to illustrate the trends and to make practical recommendations.

3.3. Permeability channel analysis

The locations of permeability channel outlets as determined by use of Mode 2 of the permeability fixture is shown in Figure 7. While the presence of channels undoubtedly affects permeability, permeability values did not always scale in proportion to the number density of channels, a counter-intuitive finding. Broadly, the LP series exhibited more channels than the HP series. In Trial 1, each LP series sample showed 8–17 channels, while the HP series

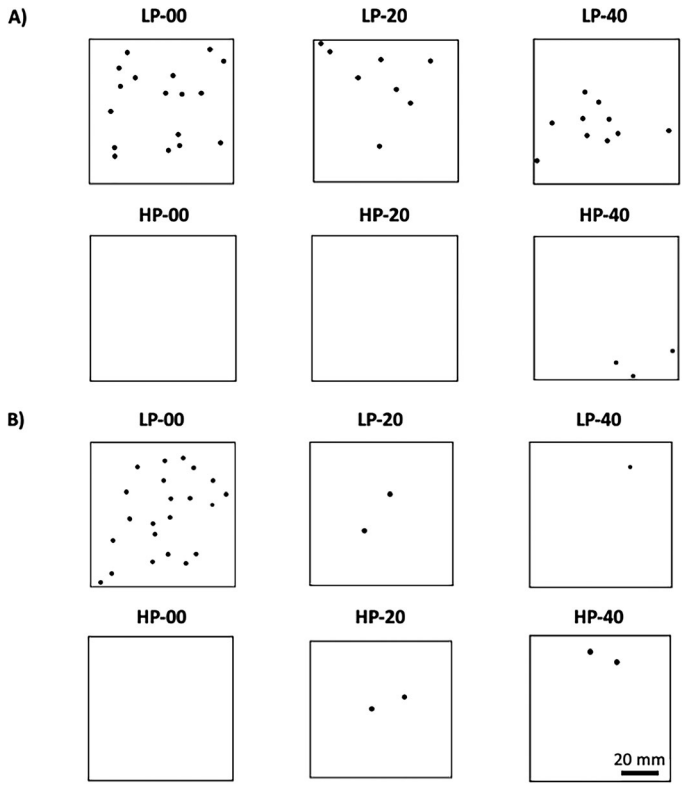

Figure 7. Permeability channel maps for (A) Trial 1 and (B) Trial 2.

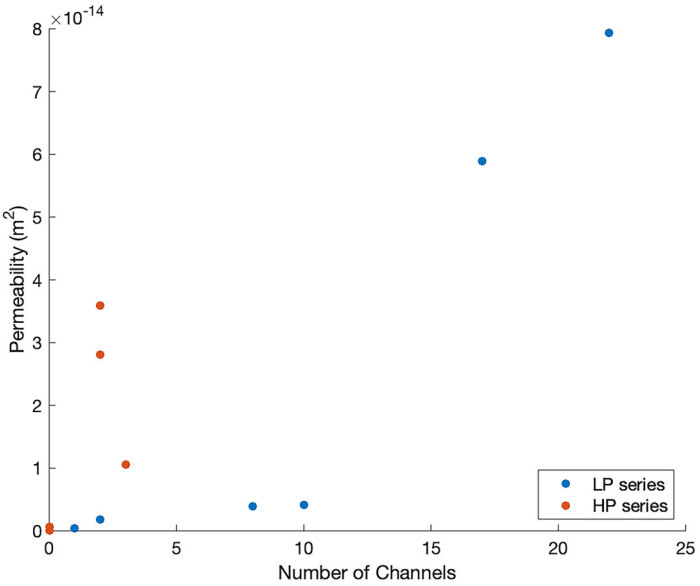

Figure 8. Number of permeability channels and permeability values compared for Trials 1 and 2.

showed 0–3 channels. Trial 2 displayed more variation in the LP series. While LP-00 contained 22 channels, LP-20 had two channels and LP-40 had one channel. In contrast, the HP series contained 0–2 channels. Pressure conditions were not sufficient to accurately predict the number of channel openings that appeared.

To further explore the character of permeability channels, the number of channels was then compared to permeability values in Figure 8. While there was not a direct relationship between channel number and permeability, having 17 or more channels was associated with the highest permeabilities, while having no channels was associated with the minimum permeabilities. However, beyond this general trend, the number of channels cannot be used to predict permeability. For example, within the HP series, the presence of two channels resulted in higher permeability than having three channels. Within the LP series, the presence of eight channels

or ten channels resulted in the approximately the same permeability. These results indicate that factors beyond number of channels affect permeability, such as the channel size and degree of connectivity. However, the effects cannot be well understood using the methods employed here, and alternative measurement methods may be required to clearly define this relationship.

3.4. Microstructural analysis

Figure 9 shows representative examples of polished sections. The micrographs provide an overview of part quality, which can be assessed by the extent of porosity, dimpling, and fillet shape/size. Samples produced with low bag pressure (LP) exhibited high porosity (>1%) in the facesheets on Sides A and B, as expected. In contrast, panels produced with high bag pressure (HP) exhibited relatively low porosity levels (<1%). Low bag pressures also yielded greater irregularities in fillet shape, a result of gas egress from the prepregs and associated foaming. Fillets were disrupted by the foaming, and in some cases were entirely absent. In contrast, fillets in HP panels exhibited smooth contours and appeared more regular in shape. Based on qualitative assessments, dimpling and fillet quality were superior in HP panels.

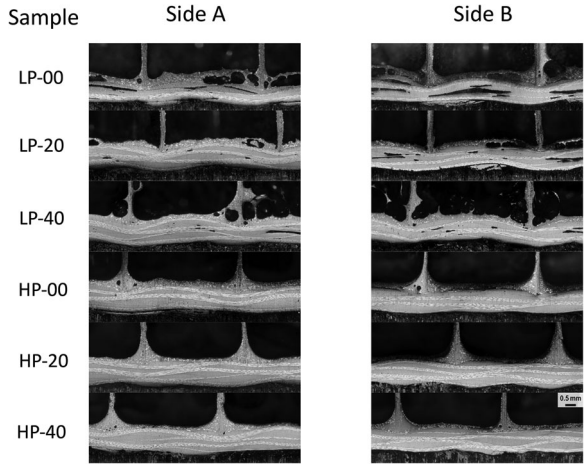

Figure 9. Representative micrographs of polished cross sections for each case.

Porosity measurements were compared to measured permeability values, as shown in Figure 10. Higher porosity levels generally were associated with higher permeabilities, but low porosity levels sometimes were associated with high permeabilities. For example, in Trial 1, LP-00 exhibited both the greatest porosity and greatest permeability, while LP-20 and LP-40 also exhibited high (but disparate) porosity levels (>2%) yet showed nearly identical permeability values. In contrast, the permeability of HP-40 was three times greater than those of LP-20 and LP-40, while the porosity was 20 times less. As a second example, in Trial 2 of the LP series, decreasing porosity led to decreasing permeability. However, the HP series showed uniformly low porosity (<1%), while permeability values spanned three orders of magnitude, ranging from 6.3×10^{-16} m^2 to 3.6×10^{-14} m^2. Summarizing, high porosity was associated with high permeability, but low porosity did not necessarily lead to low permeability. The lack of a direct correlation was attributed to intrinsic variability both in the distribution of porosity and in the techniques used to measure porosity. Polished sections provide only a local view of the microstructure and may not necessarily represent the more global porosity level within the volume of the structure.

To more accurately visualize the channel structure and to further understand the relationship between channel number, porosity, and permeability, X-ray tomograms were acquired. In Figure 11, the tomograms revealed the complexity in the channel configurations, which often included multiple channels connecting to a single opening. This degree of connectivity explains in part why the relationship between permeability and the number of channel openings is not simple, since multiple channels may connect to each opening. A supplemental video of a tomogram is also provided. Further characterization of the channel structure and analysis of the

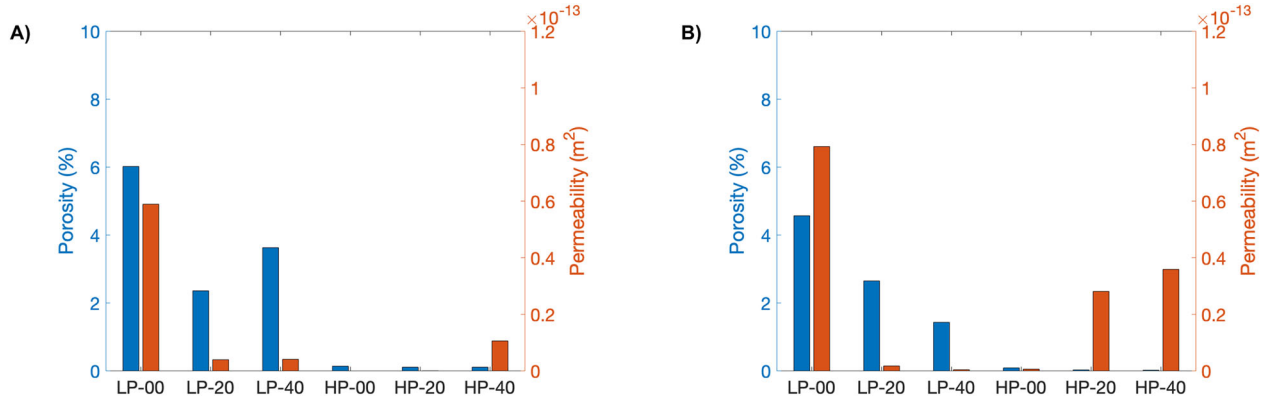

Figure 10. Porosity and permeability values compared for Trials 1 and 2.

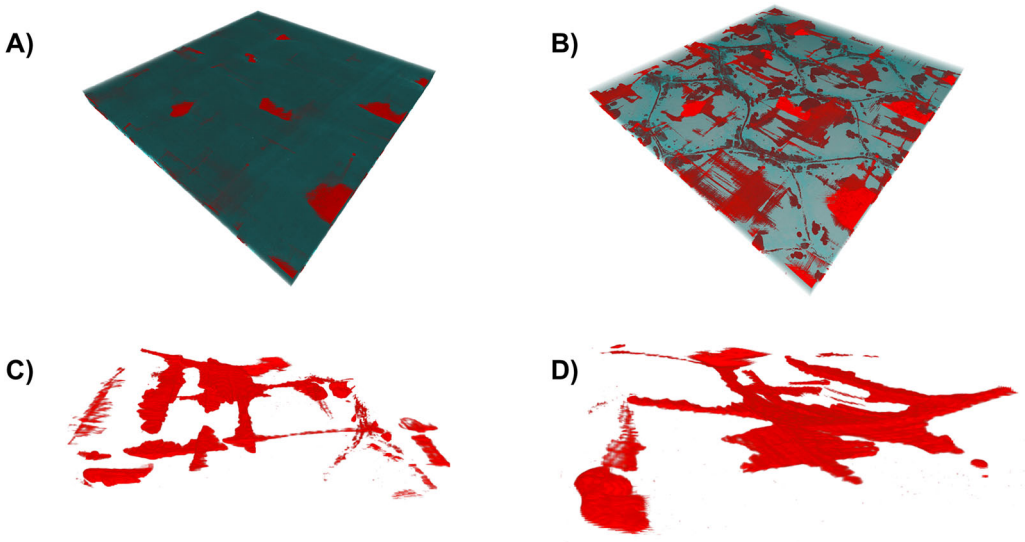

Figure 11. Representative X-ray tomogram showing interconnected channels.

tortuosity may provide additional insight into the relationship.

The findings reveal that pressure gradients strongly affect certain defect formation mechanisms that involve gas transport. With the in-bag pressurization series and the low-pressure samples with high gradients, defects were suppressed. However, for the low-pressure samples, selected core and bag pressures were insufficient (too low) to suppress void growth at exposed surfaces, especially absent pressure transfer from the autoclave. The use of in-bag pressurization reduced porosity, and permeability was reduced because channels closed prior to gelation. However, when the pressure gradient increased beyond a critical level, the gas flow increased in response, causing channels to remain open and increasing permeability. In situations where low pressure is unavoidable, a large pressure gradient may suffice to evacuate air, reduce defects, and reduce permeability.

4. Conclusions

The influence of co-cure process conditions (specifically, core and bag pressures) on the permeability of cured honeycomb skins has been determined. Experiments related two pressure-controlled factors (level of pressure and extent of gas flow through the facesheet) to gas permeability. 12 honeycomb panels were co-cured under diverse pressure conditions. Then, cured skin permeability was measured, flow was observed visually, and microstructural features were characterized using image analysis and X-ray tomography. The results provide insights into how co-cure phenomena affect permeability:

1. *Process conditions can affect permeability of cured skins.* Varying bag and core pressure conditions resulted in both high-permeability and low-permeability face sheets. Furthermore, panels with negligible skin permeability were also produced, demonstrating that production of impermeable face sheets is both possible and repeatable.
2. *Porosity in facesheets can increase permeability.* The sample with the highest porosity in the facesheet also exhibited the greatest cured skin permeability, even in the absence of a pressure difference (ΔP) across the skin during cure. The finding indicates that high levels of porosity are likely to increase permeability of cured skins, even if pressure conditions during cure do not explicitly lead to the formation of flow channels.
3. *Low porosity facesheets do not ensure impermeability.* Samples with low porosity but measurable skin permeability were produced by inducing gas flow through the skin during co-cure. The finding indicates that gas flow driven by a difference between bag and core pressures can lead to formation of flow channels in cured skins, and that internal void content sampled from cross-sections is not a comprehensive or rigorous method for estimating cured skin permeability.
4. *Cured skin permeability can be associated with a relatively small number of flow channel openings, although such openings may not be discrete flow channels.* Observation of gas flow through cured facesheets shows that even low-porosity samples can be rendered permeable by just a few (2–3)

gas flow channels sites. This observation coupled with tomographic images indicates that channel openings are not an accurate metric by which to estimate permeability.

5. *The absence of detectable flow channels indicates negligible permeability.* Samples without channels exhibited negligible permeability, indicating that the complete absence of channels can be used to estimate impermeability. A relationship exists between channels, channel openings, and permeability, even if it is not yet quantified for larger channel numbers.

For commercial production of impermeable parts, the most direct and effective strategy for co-cure of low-defect parts should rely on raising bag and core pressures to levels that suppress porosity. If in-bag pressurization is applied to equilibrated core, the lack of pressure gradient between the bag and core can prevent the driving of gases through the skin. Both the suppression of porosity and reduction of gas driven through the skin will reduce permeability. Use of in-bag pressurization in production may require modifications to autoclaves and vacuum accessories. Nevertheless, lab-scale work indicates that the approach offers a pathway to consistent fabrication of defect-free parts.

The effects of pressure as a process parameter was explored, although other factors were not considered in the experimental design. Four plies of plain-weave fabric were used for each experiment. Increasing the number of plies or using unidirectional tape is expected to change the length and character of gas flow pathways, which will in turn affect permeability. Additionally, half-sandwich structures with only the bag-side facesheet were used. The tool-side facesheet is expected to exhibit different permeability.

Additionally, not all potential factors contributing to permeability were measured. Matrix microcracking can be expected to increase permeability but would be difficult to quantify with the equipment used. However, investigating microcracking effects on permeability is undoubtedly worthwhile. Darcy's Law averages the permeability over area, yet permeability in co-cured parts can be highly localized. Localization of permeability can also be considered in the context of vented versus sealed cores. In a vented core with perforations between cell walls, a channel anywhere in the facesheet can render the whole sheet permeable. However, in sealed cores, permeability could be isolated in individual cells or facesheet locations. A model that relates permeability to discrete locations may yield clearer understanding of the process as well.

Further work is needed to clarify the mechanisms by which co-cure conditions affect the structure of permeability channels (size, shape, location), as well as the relationships between internal microstructure and permeability channels. Additional insight into these formation processes and an understanding of the physics behind them can lead to strategies and guidelines for process optimization – and, ultimately, to higher-quality and safer composite structures in aerospace and other industries.

Acknowledgements

This manuscript was written in honor of Timotei Centea, his contributions to the authors, and his contributions to the M.C. Gill Composites Center. The authors acknowledge support from NASA NRA NNL16AA13C "A Physics-Based Process Model for Co-Cure Bonding of Honeycomb Core Sandwich Structures" and from the M. C. Gill Composites Center at the University of Southern California. The author also acknowledges undergraduate research funding from the Viterbi School Merit Research Award and the Viterbi Fellows program, which allowed her to perform the work experiments and analysis described in this study. The authors acknowledge valuable discussions with project partners at NASA, the University of Delaware, and United Technologies. The authors are grateful for material donations from Hexcel (Gordon Emmerson, Yen Wang), Henkel Aerospace Materials (David Leach), Cytec Solvay (Scott Lucas, Steve Howard), the Gill Corporation (Jessie MacLeod), and Airtech International (Cole Standish).

Disclosure statement

There are no conflicts of interest to declare.

ORCID

Trisha Palit http://orcid.org/0000-0001-8521-5489
Steven Nutt http://orcid.org/0000-0001-9877-1978

References

[1] Yuan C, Li M, Zhang Z, et al. Experimental investigation on the co-cure processing of honeycomb structure with self-adhesive prepreg. Appl Compos Mater. 2008;15(1):47–59.
[2] Campbell FC, Flake C. Manufacturing technology for aerospace structural materials. Amsterdam: Elsevier; 2006.
[3] Hubert P, Poursartip A. A review of flow and compaction modelling relevant to thermoset matrix laminate processing. J Reinf Plast Compos. 1998;17(4):286–318.
[4] Darcy H. Les Fontaines Publiques de la Ville de Dijon. Paris: Dalmont; 1856.
[5] Tavares SS, Caillet-Bois N, Michaud V, et al. Vacuum-bag processing of sandwich structures: Role of honeycomb pressure level on skin–core adhesion and skin quality. Compos Sci Technol. 2010;70(5):797–803.

[6] Kratz J, Hubert P. Evaluation of core material on skin quality for out-of-autoclave honeycomb panels. Proc. SAMPE 2012 Conf. Baltimore: Society for the Advancement of Materials and Process Engineering; 2012.
[7] Kratz J, Hubert P. Vacuum bag only co-bonding prepreg skins to aramid honeycomb core. Part I. Model and material properties for core pressure during processing. Compos Part A Appl Sci Manuf. 2015;72:228–238.
[8] Tavares SS, Michaud V, Månson JAE. Through thickness air permeability of prepregs during cure. Compos Part A Appl Sci Manuf. 2009;40(10):1587–1596.
[9] Tavares SS, Caillet-Bois N, Michaud V, et al. Non-autoclave processing of honeycomb sandwich structures: Skin through thickness air permeability during cure. Compos Part A Appl Sci Manuf. 2010;41(5): 646–652.
[10] Grenoble RW, Gates TS. Hydrogen gas leak rate testing and post-testing assessment of microcrack damaged composite laminates. AIAA/ASME/ASCE/AHS/ASC Structures, Structural Dynamics, and Materials Conference; 2006.
[11] Kratz J, Hubert P. Anisotropic air permeability in out-of-autoclave prepregs: Effect on honeycomb panel evacuation prior to cure. Compos Part A Appl Sci Manuf. 2013;49:179–191.
[12] Kratz J, Hubert P. Vacuum-bag-only co-bonding prepreg skins to aramid honeycomb core. Part II. In-situ core pressure response using embedded sensors. Compos Part A Appl Sci Manuf. 2015;72:219–227.
[13] Centea T, Zebrine D, Anders M, et al. Manufacturing of honeycomb core sandwich structures: Film adhesive behavior versus cure pressure and temperature. CAMX 2016 - Composites and Advanced Materials Expo; 2016.
[14] Anders M, Zebrine D, Centea T, et al. In situ observations and pressure measurements for autoclave co-cure of honeycomb core sandwich structures. J Manuf Sci Eng. 2017;139(11):1–9.
[15] Kim D, Centea T, Nutt SR. Out-time effects on cure kinetics and viscosity for an out-of-autoclave (OOA) prepreg: Modelling and monitoring. Compos Sci Technol. 2014;100:63–69.
[16] Technologies CM. Cytec FM309-1 material properties characterization; 2013.
[17] Howard SJ. Evaluating consolidation dynamics-study of key consolidation parameters in a vacuum bag only (VBO) cure. International SAMPE Technical Conference; 2016.
[18] Palit T, Centea T, Anders M, et al. Permeability of cured composite skins produced using co-cure over honeycomb core. Proc. CAMX 2018 (Student Compet); 2018.
[19] Centea T, Simacek P, Anders M, et al. Understanding and modeling the co-cure of honeycomb core sandwich structures. International SAMPE Technical Conference; 2019.
[20] Kermani NN, Simacek P, Advani SG. A model for the equilibrated co-cure of honeycomb core sandwich structures in autoclave processing. Proceedings of the American Society for Composites; 2019.
[21] Anders M, Zebrine D, Centea T, et al. Process diagnostics for co-cure of sandwich structures using in situ visualization. Compos Part A Appl Sci Manuf. 2019;116:24–35.
[22] Epstein G, Ruth S. Honeycomb sandwich structures: Vented versus unvented designs for space systems. Int J Solids Struct. 1993;1–21.
[23] Brand RA, Brown GG, McKague EL. Processing science of epoxy resin composites. San Diego (CA): General Dynamics Convair Div; 1984.
[24] Hexcel Composites. Product data HexPly 8552. Hexcel; 2000.
[25] Henkel Aerospace. LOCTITE EA 9658 AERO epoxy film adhesive - Technical Process Bulletin; 2013.